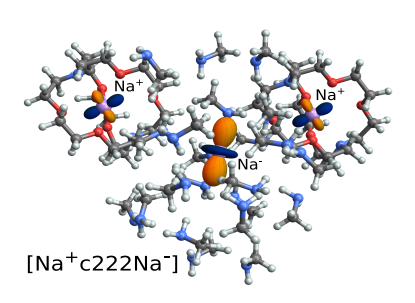
The Sodium Anion Is Strongly Perturbed in the Condensed Phase Even Though It Appears Like a Free Ion in Nuclear Magnetic Resonance Experiments

Laura Abella, Adam Philips, and Jochen Autschbach*

Department of Chemistry
University at Buffalo
State University of New York
Buffalo, NY 14260-3000, USA
email: jochena@buffalo.edu

Abstract: Solvated sodium anions (Na⁻) were thought to behave essentially like isolated gas phase ions that interact only weakly with their environments. For example, ²³Na NMR signals for solvated Na⁻ are very sharp, despite the potential for strong quadrupolar broadening. The sharp NMR signals appear to indicate a nearly spherical electron density of the ion. For the present study, abinitio molecular dynamics simulations and quadrupolar relaxation rate calculations were carried out for the Na⁻ / Na⁺ [2.2.2]cryptand system solvated in methylamine, followed by detailed analyses of the electric field gradient at the sodium nuclei. It is found that Na⁻ does not behave like a quasi-free ion interacting only weakly with its environment. Rather, the filled 3s shell of Na⁻ interacts weakly with the ion's own core and the nucleus, causing Na⁻ to appear in NMR experiments like a free ion.



Alkali metals are well known for their strong tendency to form positive ions. The spectacle of alkali metals reacting with water is a favorite chemical demonstration. It is less well known that these elements can also accept an electron, forming the corresponding negative *alkalide* ions.¹ There is high interest in solutions of alkalides as they can act as strong reducing agents in the production of nanoscale metal particles, organic synthesis, intermetallics and colloidal metals. Due to their fascinating properties, numerous studies of alkalide ions and related systems have been carried out.^{2–10} For example, reacting alkali metal solutions with cryptands has led to the discovery of crystalline salts of complexed alkalide ions. Ceraso *et al.* isolated and characterized Na⁺/Na⁻ salts with the 2.2.2 cryptand, viz [Na⁺ [2.2.2]cryptand Na⁻],^{11,12} which has been

thoroughly characterized. We abbreviate this system as [Na⁺c222Na⁻] in the following.

NMR spectroscopy provided the first unequivocal proof of the existence of alkalide ions in solutions and solids. 11-15 The resolution of the NMR experiment allows for the simultaneous identification of both the anion and the complexed cation. For instance, ²³Na NMR chemical shifts have been measured for [Na⁺c222Na⁻] on several occasions.^{4,12,16,17} The chemical shift of Na⁺ in this system is typical of the shift detected for other sodium salts. The cation is inside the cryptand and isolated from the alkalide ion and the solvent, if present. Therefore, the Na⁺ chemical shift is nearly solvent independent. For Na, the observed chemical shift was reported to be almost the same as one calculated for the gas phase anion¹⁶ and also essentially independent of the solvent. Other alkali metal anions have also been synthesized with the [2.2.2]cryptand, such as K⁻, Rb⁻, and Cs⁻. The metal NMR data showed a stronger sensitivity to the chemical environment for these metals. 4,9,12,18 Experimental investigations concluded that Na is a 'genuine' anion in which both the [Ne] core and the 3s valence electrons interact very weakly with their surroundings. 16,17,19 Strong evidence for this characterization was provided by the almost complete absence of quadrupolar broadening of the ²³Na NMR signals. A quadrupolar broadening would arise from an electric field gradient (EFG) generated in Na by a distortion of its electron density, and by the presence of fluctuating non-spherical partial charge distributions from other ions and solvent molecules in the surrounding. The extremely narrow observed widths of the Na NMR signals suggests the lack of an EFG, and a spherical symmetry of these species.

However, the Na⁻ ion is strongly polarizable. We estimate its gas-phase isotropic static polarizability to be over 800 times that of Na⁺ (808 vs. 1 atomic units (au), PBE/ATZP, computational details provided below), similar to previous reports.²³ In order to highlight the comparison between Na⁺ and Na⁻, we calculated the radial electron probability densities $D(r) = r^2 \rho(r)$ for Na⁻ and Na⁺, shown in Figure 1. The outermost radial density peak of Na⁻ is just above 2 Å, with a pronounced tail toward larger r, indicating the extension of the 3s shell. This result is in accordance with other estimates of the Na⁻ radius. For example, Matalon *et al.*²⁴ estimated a radius of ~2.25 Å and Tehan *et al.*⁵ reported a value of 2.10 Å.

It is inconceivable that the diffuse and easily polarizable 3s shell of Na¯ does not get perturbed strongly by the environment in a solution or a solid. The lack of a pronounced NMR quadrupolar line broadening, despite the huge polarizability of Na¯, suggests that the filled 3s shell interacts only very weakly with the [Ne] 1s²2s²2p⁶ core such that the 3s polarization is not 'felt' at the nucleus in terms of a sizable EFG. The filled 3s shell may also serve as a spatial buffer to shield the [Ne] core from being polarized itself, and prevent surrounding charges to come close, with a concomitant lack of an EFG at the ²³Na nucleus that would otherwise broaden the NMR signal. Computational quadrupolar NMR spin relaxation studies based on force-field and ab-initio molecular dynamics (FFMD, aiMD) have been carried out for Na¯+,25–29 but little is known from such

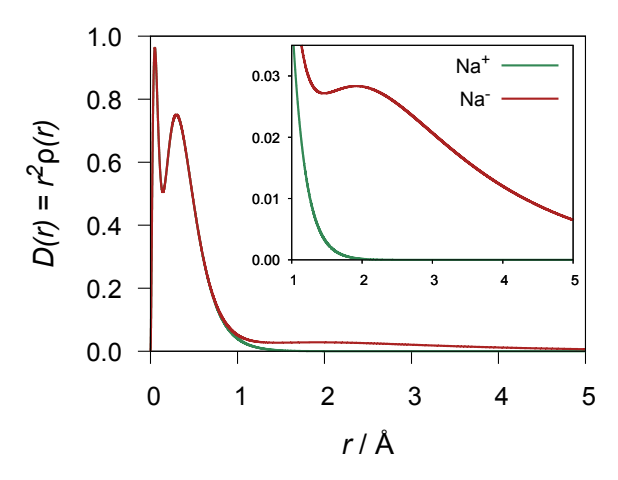


Figure 1: Radial electron density of Na cation (green line) and Na anion (red line). Inset: region of the 3s shell. The outermost maximum for the anion is just above 2.00 Å.

theoretical approaches about Na⁻. For the present study, we probed the above hypotheses with a combination of aiMD of [Na⁺c222Na⁻] solvated in methylamine and calculations of the timedomain EFG tensors, the quadrupolar relaxation rates, and analyses of the EFG tensor components in terms of contributions from core and valence shell localized molecular orbitals.

The theoretical framework for nuclear spin relaxation used here is discussed, for instance, in Refs. 20–22. The calculation of quadrupolar relaxation via aiMD simulations³⁰ was implemented by us as detailed in refs. 27, 29, 31. For brevity, we only provide the key steps here. Calculations of EFG tensors along the aiMD trajectory provides the auto-correlation functions (ACFs) $f_{2,m}(\tau) = \langle R_{2,m}^*(t) R_{2,m}(t+\tau) \rangle$ of the time-domain rank-2 EFG spherical tensor components $R_{2,m}(t)$. The brackets indicate an ensemble average that is replaced in numerical simulations by ACF calculations for a discrete set of time steps. In the fast-motion ('extreme narrowing') limit, which applies to our system, the $f_{2,m}(\tau)$ are converted to quantities $g_{2,m}$ via taking half-Fourier transforms in the limit $\omega \to 0$. Under rotational isotropy, for solutions, the $f_{2,m}(\tau)$ and $g_{2,m}$ for different m become equal, and the longitudinal and transverse relaxation rates likewise become equal. An isotropic relaxation rate $1/T_{\rm iso} = 1/T_1 = 1/T_2$ can then be formulated as

$$\frac{1}{T_{\rm iso}} = 2C^{Q} \tau_{c} \langle V(0)^{2} \rangle \quad ; \quad \tau_{c} = \frac{1}{\langle V(0)^{2} \rangle} \sum_{m=-2}^{2} g_{2,m} \tag{1}$$

Here, $\langle V(0)^2 \rangle = \sum_m f_{2,m}(0)$ is the total EFG variance, and τ_c is a corresponding autocorrelation time associated with the relaxation. Rotational isotropy can be difficult to establish in numerical simulations,²⁹ which by their nature sample the system incompletely. Therefore, the $f_{2,m}$ and $g_{2,m}$ were calculated for different m first and then averaged as in the eq. (1), rather than assuming that

they are equal. Calculations of $1/T_1$ and $1/T_2$ from the full formalism²⁰ and comparison with $1/T_{\rm iso}$ then gives a rough estimate of the sampling errors as far as a lack of rotational isotropy is concerned. For this work, half-height NMR line widths were computed according to

$$\Delta v = \frac{1}{\pi T_2} \tag{2}$$

Car-Parrinello (CP) aiMD simulations were carried out using Quantum-Espresso (QE) version 6.0.^{32,33} Following previous studies^{27,29,31,34} the exchange-correlation functional of Becke, Lee, Yang and Parr (BLYP)35,36 and ultrasoft pseudopotentials were selected for these simulations,³⁷ along with semi-empirical dispersion corrections.³⁸ The mass of deuterium was used for all hydrogens atoms to facilitate adiabatic separation between electronic and nuclear degrees of freedom.³⁹ A kinetic energy cutoff of 100 Ry was chosen for the plane-wave basis, along with a fictitious electron mass of 450 au and a time step of 5 au (corresponding to 0.121 fs), similar to previous studies.^{27,40,41} The aiMD simulations were performed with the Verlet algorithm. The X-ray crystal structure of [Na⁺c222Na⁻] was packed in a cubic cell together with 24 methylamine molecules, using Tinker.⁴² The box dimensions were 12.71 Å, such that the density of the system was that of methylamine at ambient conditions (0.7 g/cm³). The initial packing structure was optimized prior to starting the first aiMD simulation. Random configurations ('snapshots') generated from the trajectory were then used to spawn new independent trajectories upon heating and re-equilibration. For each trajectory, the system was heated to the temperature of the experiments (258 K) using a three-chain Nosé-Hoover thermostat (90.0, 45.0, 15.0 THz). The aiMD simulations were equilibrated for 2.5 ps in NVT, then continued in NVE. Excluding the first ~1 ps in NVE, the remaining portions of the simulations comprise the production phases of the trajectories. The total production time for each simulation was around 20 ps. All dynamics were stable in NVE.

For continuity with previous work on quadrupolar relaxation by our group, ^{27,29,31} and for comparison, we also performed a set of ten simulations using the exchange-correlation functional of Perdew, Burke, and Ernzerhof (PBE). ⁴³ Further details regarding these computations and other test calculations can be found in the Supporting Information (SI).

EFG computations were performed for 1000 evenly spaced snapshot configurations along the production phase of a simulation using the gauge-including projector-augmented wave (gipaw) module of QE,^{32,44} with periodic boundary conditions and the PBE functional. We refer to these calculations by the 'PAW' acronym. A small-core pseudopotential for sodium was utilized, with the 2s and 2p shells included in the valence space. A reimplementation of our DynPro ('dynamic properties') relaxation rate module for the QE package,²⁷ was used for the relaxation rate calculations. An open source tool developed in our group (version 0.3.11)⁴⁵ was employed to analyze

trajectories, extract cluster configurations, and perform visualizations.

Additional calculations of EFG tensors, ion polarizabilities (vide supra), and the electron densities of Figure 1 were performed with non-periodic boundary conditions, PBE, and all-electron Slater type orbital (STO) basis sets, using the Amsterdam Density Functional (ADF) 2017 package. We denote these calculations as 'STO'. In selected cases the PBE0⁴⁷ hybrid functional (25% exact exchange) was employed for comparison. A triple- ζ polarized basis (TZP) augmented with diffuse functions (ATZP) was used for sodium (TZP for Na⁺ in subsequent analyses), and a double- ζ polarized STO basis (DZP) for all other atoms. Solvent effects beyond those furnished by the finite [Na⁺c222Na⁻] - methylamine clusters of varying size extracted from the MD trajectories were treated by means of the continuous conductor-like screening model (COSMO)⁴⁸ with a dielectric constant for methylamine of 9.4. An example snapshot is shown in Figure S1 in the SI.

A previous computational study of $[M(en)_3^+M^-]$ ion pairs, with M= alkali and en= ethylene-diamine, showed that the ion charges calculated with the non-hybrid PBE functional are not ± 1 but closer to about ± 0.6 . Test calculations (see SI) demonstrate that the Kohn-Sham delocalization error (DE)^{49,50} is partly responsible for these reduced ion charges. A long-range corrected hybrid functional, tuned to minimize the DE,⁵¹ places the charges closer to ± 0.7 , with results from the PBE0 global hybrid being close. However, the calculated sodium EFGs are not strongly affected by choosing different functionals, and Kohn-Sham calculations of EFGs are known to perform generally quite well for main group elements.⁵² Since the relaxation rate calculations require a large number of EFG calculations, and benefit from the periodic PAW approach, we determined that the PBE-based relaxation rate calculations and subsequent analyses are sufficiently accurate for the purpose of this study. This is in line with comparisons between PAW and STO, and between PBE and PBE0, performed by us previously for EFGs and quadrupolar relaxation of main group elements including ²³Na,²⁹ and present test calculations (see SI).

We show in the following that the calculated relaxation rates are in agreement with experimental findings in that Na⁻ has a very small quadrupolar broadening for solvated [Na⁺c222Na⁻], even much smaller than the encapsulated 'hard' ion Na⁺. The EFGs are analyzed subsequently, in conjunction with the orbital occupations, in order to rationalize this unintuitive finding for Na⁻.

A summary of relaxation data obtained with the non-hybrid functional PBE from fifteen trajectories is provided in Table 1. Table S2 shows the data for the individual trajectories. Sampling errors were probed by performing independent trajectories. The absolute difference between $1/T_1$ and $1/T_2$ is larger for the Na cation than the anion, but on a relative scale the differences are comparable. $1/T_{\rm iso}$, as calculated from Equation (1), is seen to lie in between $1/T_1$ and $1/T_2$. The differences may serve as a rough estimate of the finite-system finite-time sampling errors. Given the finite time scales of the simulations relative to the relaxation phenomenon, nonequivalent

 $1/T_1$ and $1/T_2$ suggest somewhat anisotropic sampling in the fast motion regime. Overall, the calculated isotropic relaxation rate $1/T_{\rm iso}$ for Na⁺ is about ten times larger than for Na⁻, with a corresponding ratio in the line widths Δv .

The experimental NMR line widths of Na ions in a methylamine solution of [Na⁺c222Na⁻] at -15°C were first reported by Dye *et al.* to be 11 Hz for Na⁻ and 30.8 Hz for Na⁺. Our calculated line widths are smaller for Na⁻. However, Dye et al. noted the difficulty of obtaining the true quadrupole-broadened line width because of the presence of solvated electrons and the concomitant paramagnetic interactions. Subsequently reported experimental widths of Na⁻ signals were as low as a single hertz in some instances, in measurements with alternative solvents such as ethylamine at -17°C to 1°C and tetrahydrofuran at -4°C, or for related systems such as Na⁺(18-Crown-6)Na⁻ and Na⁺(12-Crown-4)Na⁻. ^{12,15,18} Therefore, our calculated data are within the experimentally observed range for Na⁻. Moreover, in agreement with experimental observations, the Na⁻ lines are only very weakly broadened by quadrupolar relaxation.

According to eq. (1), $1/T_{\rm iso}$ is proportional to the product of τ_c and $\langle V(0)^2 \rangle$. The calculations show that the total EFG variance $\langle V(0)^2 \rangle$ for Na⁺ is almost three times higher than for Na⁻. The correlation time and the variance both contribute to the lower rate for the anion. Evidently, the diffuse polarizable 3s shell of Na⁻ does not cause systematically larger $\langle V(0)^2 \rangle$ when compared to the 'hard' (weakly polarizable) Na⁺ ion. The EFG autocorrelation functions (ACFs) f_{2m} , are shown in Figure 2. After an initial very fast decay, known as the libration region, the decay of the f_{2m} for Na⁺ takes much longer than for Na⁻, which causes the much larger τ_c for the former. In our MD trajectories, Na⁻ does not tend to form coordination motifs with the solvent and/or cryptand containing the cation that are long-lived compared to the correlation time spans, i.e. the anion appears to be fully solvated in an environment that fluctuates considerably over the relaxation correlation time spans. Coordinated Na⁻ species were not apparent from visual inspections of our trajectories,

Table 1: ²³Na NMR relaxation data* for a set of fifteen solvated [Na⁺c222Na⁻] trajectories at 258 K.

		$\frac{1}{T_1}$	$\frac{1}{T_2}$	$rac{1}{T_{ m iso}}$	$ au_c$	$\langle V(0)^2 \rangle$	$\Delta \nu$
Average	Na ⁻	9.88	8.77	9.14	0.75	0.44	2.79
	Na^+	84.27	99.21	94.23	4.49	1.22	31.58
Standard	Na ⁻	4.56	3.46	3.80	0.18	0.12	1.10
Error	Na ⁺	12.54	15.04	13.84	0.56	0.07	4.79

^{*} Calculated values with 24 molecules per simulation cell. EFGs were computed for 1000 snapshot clusters from the aiMD BLYP simulations. b EFGs computed using PAW/PBE. All quantities are averaged over a set of 15 trajectories. Relaxation rates and line widths are in Hz, τ_c is in ps, and $\langle V(0)^2 \rangle$ is in atomic units %. Experimental line width of Na⁺is three times larger than Na⁻.

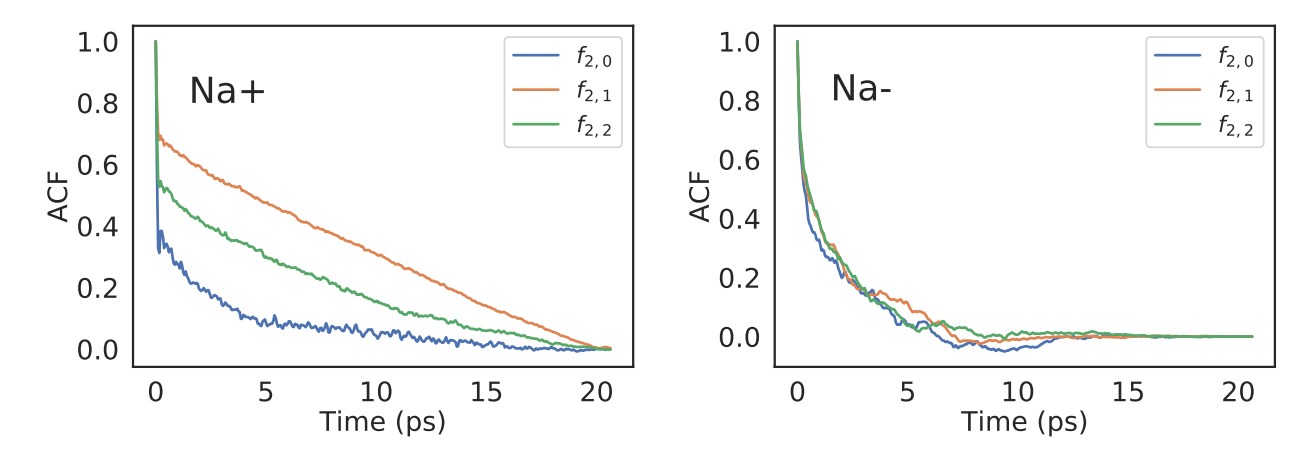


Figure 2: Autocorrelation functions (ACFs) of the second rank irreducible tensor components of the electric field gradient (EFG) averaged over the sodium atoms of the 15 trajectories. EFG computed using PAW method.

likely because the anion is too diffuse and 'squishy' to form transient complexes. Thus, it would seem to be a permissible approximation to employ the simulation cell sizes that we use. A series of structural and dynamic analyses were performed to rationalize the slow decorrelation of Na⁺ (see SI). Trajectories with larger correlation times exhibit a limited range of motion, or motion within one side of the cryptand cavity. The resulting spherical asymmetry and sluggishness of the cation motion results in the slow decorrelation and inequivalence of the components of the EFG tensor in Figure 2. It is always possible that a process that is longer than the simulation time influences the relaxation. However, it is not practical to extend the simulations to a point where this concern could not be raised. Our good agreement with the experimental line widths indicates that slower processes are likely not a major influence on the sodium ion relaxation, and that the relevant dynamics are captured reasonably well.

We originally performed simulations of the 23 Na NMR relaxation rates with the PBE functional (see SI for more details), at a substantially elevated temperature (320 K) out of an abundance of caution due to known problems of this functional with the structure of liquid water, 39,53 even though it is unclear if the methylamine solvent structure is impacted in the same way. The PBE-based line width for Na $^-$ (1.72 \pm 0.43 Hz) is a bit smaller than the BLYP-based result, but within the latter's standard error. The relaxation rates for the Na $^+$ ion differ by much more than the standard errors, and the rate with the elevated PBE simulation temperature (7.28 \pm 2.12 Hz) is too low compared to the experimental 30.8 Hz reported by Dye et al. Clearly, the elevated temperature causes a too fast and too large ranged motion of Na $^+$ inside the cryptand, leading to a faster averaging of the fluctuating fields.

A detailed analysis of the EFG can be obtained from the STO calculations.⁵⁴ In order to apply the analysis to the [Na⁺c222Na⁻] system, it is important to establish that the finite-cluster STO

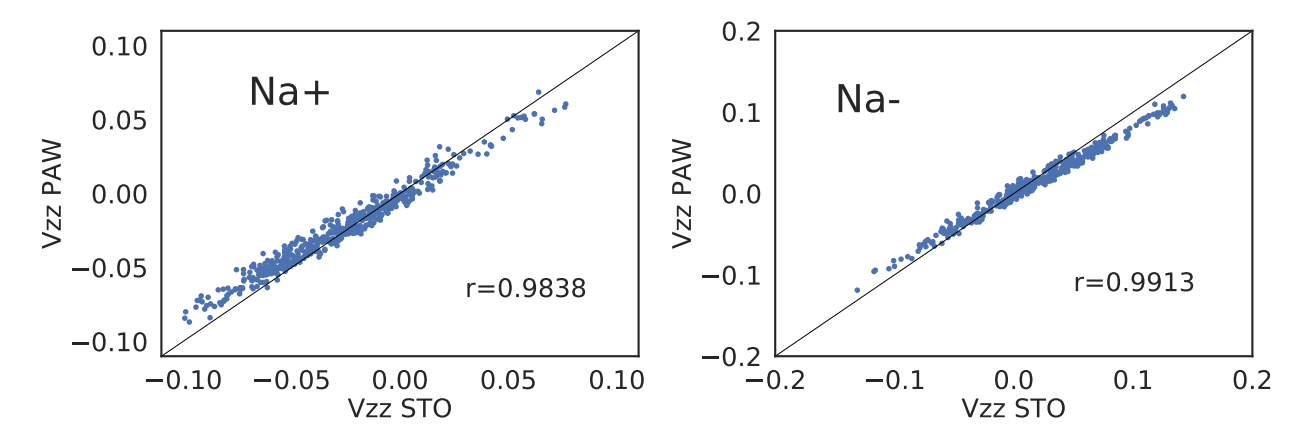


Figure 3: V_{zz} EFG component (au) at 23 Na⁺ and 23 Na⁻ nuclei for one of the trajectories. PAW vs. STO calculations with PBE functional. The straight line indicates where PAW = STO. Correlation coefficients r are given inside the plot panels.

calculations produce comparable EFGs as the infinite-periodic PAW calculations. Figure 3 shows the EFG component V_{zz} for Na⁺ and Na⁻ computed by the PAW and STO models for one of the trajectories. For both types of sodium ions, PAW gives a comparable, if slightly smaller, range of EFGs than the all-electron STO calculations. (It is a coincidence that for this particular trajectory Na^+ samples a slightly wider range of negative than positive V_{zz} .) We tentatively attribute the apparent slope of less than one for the PAW vs. STO data to the very different approximations made in the two sets of calculations, such as projector vs. all-electron, plane-wave vs. STO valence basis, and periodic boundary conditions vs. finite clusters. Given that each of these factors could strongly impact the EFG calculations, the agreement is overall very favorable. Since the EFG range in the PAW calculations is smaller than in the STO calculations we did not apply a scaling factor of 0.893 recommended in refs. 55, 56 to reduce the magnitude of PAW-based Na⁺ EFGs. Furthermore, we confirmed for three trajectories that the ²³Na NMR relaxation data obtained from PAW and STO calculations are comparable (Table S5). The tendency for the STO calculations to generate a somewhat larger EFG range translates into larger $\langle V(0)^2 \rangle$ and Δv , but the trends across the trajectories are preserved between PAW and STO calculations, also for the τ_c . We proceed with an analysis of the EFGs for selected snapshots.

EFG tensors for the sodium ions in the solvated [Na $^+$ c222Na $^-$] system were analyzed in terms of contributions from natural bond orbitals (NBOs) obtained with the NBO 5.0 program. We focus on the largest-magnitude EFG tensor component, V_{33} , which determines the nuclear quadrupole coupling constant C_Q . Table 2 summarizes the analysis. The EFG analysis is (human) time-consuming and therefore had to be limited to ten snapshots randomly selected from three of the aiMD trajectories. Table 2 also provides additional information extracted from the NBO calculations that help in interpreting the EFG analysis. The NBOs constitute a set of ideally localized

'chemist's orbitals' representing individual lone pairs, bonds, and core shells, with associated electron populations that may be integer or not. In order to assist the analysis, we list the populations of the sodium 3s NBOs as well as the total electron count from the natural population analysis. Each doubly occupied natural localized MO (NLMO) has an assigned 'parent NBO'. If the weight of the parent NBO in the NLMO is much less than, say, 95%, then the NLMO is significantly

Table 2: EFG and NBO data for selected trajectory snapshots. [a]

Table 2: EFG and NBO data for selected trajectory snapshots. ¹⁴³											
Snapshot #	1	2	3	4	5	6	7	8	9	10	
Na^+ analysis V_{33}										<u> </u>	
2p	-0.082	-0.106	-0.083	0.047	0.082	-0.059	0.094	0.043	-0.088	-0.077	
3s	0.000	0.001	0.001	0.000	0.000	0.000	0.000	0.000	0.000	0.001	
Σ 2p,3s	-0.082	-0.105	-0.082	0.047	0.082	-0.059	0.094	0.043	-0.088	-0.076	
$Diffuse^{[b]}$	-0.013	-0.015	-0.010	0.013	0.020	0.000	0.021	0.016	-0.013	-0.013	
Other $[c]$	-0.028	-0.025	-0.020	0.012	0.019	-0.007	0.022	0.008	-0.024	-0.025	
Σ analysis ^[d]	-0.123	-0.145	-0.112	0.072	0.121	-0.087	0.137	0.067	-0.125	-0.114	
Total calcd.	-0.121	-0.141	-0.109	0.071	0.116	-0.090	0.132	0.066	-0.123	-0.111	
Na $^-$ analysis V_{33}											
2p	-0.013	0.000	0.006	-0.007	-0.018	-0.008	-0.001	-0.085	-0.160	0.101	
3s	-0.006	0.003	-0.007	0.001	0.002	-0.003	0.003	-0.022	-0.049	0.026	
Σ 2p,3s	-0.019	0.003	-0.001	-0.006	-0.016	-0.011	0.002	-0.107	-0.209	0.127	
$Diffuse^{[b]}$	-0.003	0.000	-0.009	0.014	0.000	-0.009	0.007	-0.036	-0.072	0.044	
Other $[c]$	0.005	0.000	-0.002	0.004	-0.003	-0.005	0.000	-0.025	-0.031	0.027	
Σ analysis ^[d]	-0.017	0.006	-0.012	0.012	-0.019	-0.025	0.009	-0.168	-0.312	0.198	
Total calcd.	-0.017	0.006	-0.012	0.013	-0.019	-0.025	0.009	-0.162	-0.293	0.196	
NBO populations[[e]										
Na ⁺ 3s	0.091	0.094	0.092	0.085	0.088	0.089	0.090	0.090	0.105	0.106	
$Na^{-}3s$	1.622	1.709	1.590	1.645	1.581	1.635	1.628	1.475	1.369	1.364	
Composition of the 3s NLMO of Na											
% 3s NBO ^[f]	81.4	85.6	79.9	82.3	79.0	82.0	81.5	74.4	69.1	68.9	
% p	0.49	0.23	0.65	0.10	0.08	0.43	0.24	1.11	1.36	1.57	
% d	0.01	0.00	0.02	0.01	0.03	0.01	0.01	0.02	0.01	0.01	
Total natural populations											
Na ⁺	10.162	10.167	10.157	10.146	10.152	10.153	10.162	10.152	10.185	10.185	
Na ⁻	11.659	11.738	11.633	11.675	11.612	11.671	11.663	11.524	11.425	11.421	

[a] PBE STO calculations. All EFG data in au. V_{33} contributions from Na 2p, Na 3s, diffuse Na centered NBOs, and contributions from other atoms are listed. Analysis according to Reference 54. One au of field gradient is approximately $9.717 \cdot 10^{21}$ V/m² and corresponds to a nuclear quadrupole coupling constant of 235.0 MHz per barn of nuclear quadrupole moment cross section. [b] Sum of contributions from diffuse Na-centered NBOs ('Rydberg' NBOs). [c] Sum of contributions larger than 1% of $|V_{33}|$ from other atoms. [d] Sum of all NBO contributions with a print threshold above 1% of $|V_{33}|$. [e] The populations are 1.999 or greater for each of the 2p orbitals. [f] Weight of 'parent NBO' 3s in the NLMO. The p and d weights are for the Na-centered part of the NLMO. The weight of s is 98% or higher and not printed individually.

delocalized. Table 2 lists the weight of the parent 3s NBO in the 3s NLMO of Na⁻, along with the weight of Na-centered p and d angular momenta in the 3s NLMO, in order to assess its degree of polarization.

The EFG tensor component V_{uv} , with $u, v \in \{x, y, z\}$ chosen to coincide with the EFG principal axis system, at a nucleus located at R_A is calculated in au as

$$V_{uv} = \int \rho(\mathbf{r}) \left[\hat{V}_{uv}(\mathbf{r}, \mathbf{R}_A) - \sum_{B \neq A}^{\text{Nuclei}} \frac{Z_B}{N} \hat{V}_{uv}(\mathbf{R}_B, \mathbf{R}_A) \right] dV$$
 (3)

Here, $\hat{V}_{uv}(\boldsymbol{p},\boldsymbol{q}) = \delta_{uv}|\boldsymbol{p}-\boldsymbol{q}|^{-3} - 3(p_u-q_u)(p_v-q_v)|\boldsymbol{p}-\boldsymbol{q}|^{-5}$ is the traceless quadrupole operator, N is the number of electrons, and Z_B the charge of another nucleus. In the analysis, the electron density $\rho(\boldsymbol{r})$ is then partitioned into densities from individual NBOs. The contributions to the EFG from other nuclear charges are absorbed in the NBO analysis weighted by the electron density, as shown above. The contributions of partial charges in the system to the sodium EFGs then show up in the analysis as contributions from NBOs centered on the relevant atoms, which show up in Table 2 in the 'Diffuse' and 'Other' rows. In 'Other', contributions from distant partial charges amounting each to less that 1% of the V_{33} magnitude were not printed and neglected. The combined influence of the neglected contributions is seen in Table 2 by comparing the rows ' Σ analysis' with 'Total calcd.' In all cases, the differences are minor.

For the Na⁺ ion the analysis reveals the following: The electron density partitioning furnished by the NBO calculation assigns an excess of 0.2 electrons (e) to the formal electron count of 10, with about 0.1e assigned to the 3s NBO, as a result of a polarization of the cryptand orbitals toward the ion and minor transfer of charge. Despite a non-negligible population, the 3s shows essentially no contribution to the EFG. The sum of the contributions of diffuse orbitals assigned to Na⁺, and other NBOs, accounts for the EFG generated by partial charges mainly in the cryptand, which provides approximately one-third to one-half of V_{33} for most snapshots. The remaining, mostly dominant, contribution comes from the Na⁺ 2p shell and must be attributed to core polarization by the surrounding partial charges.

The matching signs of the core polarization and partial charge (Diffuse + Other) contributions may be rationalized as follows: Suppose that Na⁺ is at the coordinate origin and placed between a pair of partial charges q located at $\pm a$ along the x axis. The resulting EFG, according to Equation (3), is $V_{xx} = 4q/a^3$, $V_{yy} = V_{zz} = -2q/a^3$, with $V_{xx} = V_{33}$ positive / negative if q is positive / negative. We expect positive partial charges to polarize the $2p_x$ electron density toward them, as illustrated in Figure 4. This creates a slight electron deficiency along x closer to the Na nucleus and a positive V_{33} reinforcing the positive EFG generated by the partial charges. A pair of negative partial charge would have the opposite effect.

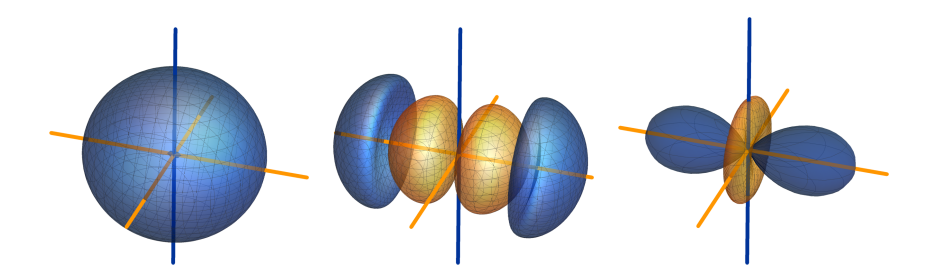


Figure 4: Left: Iso-surface of a model electron density for the Na 2p shell, polarized outward along the x axis (left to right). Center: Iso-surface plot of the corresponding deformation density relative to a spherical 2p shell. Blue (dark) indicates accumulation of electron density, orange (light) indicates depletion. Right: Polar plot⁵⁴ of the resulting EFG tensor, with blue / orange indicating positive / negative EFG.

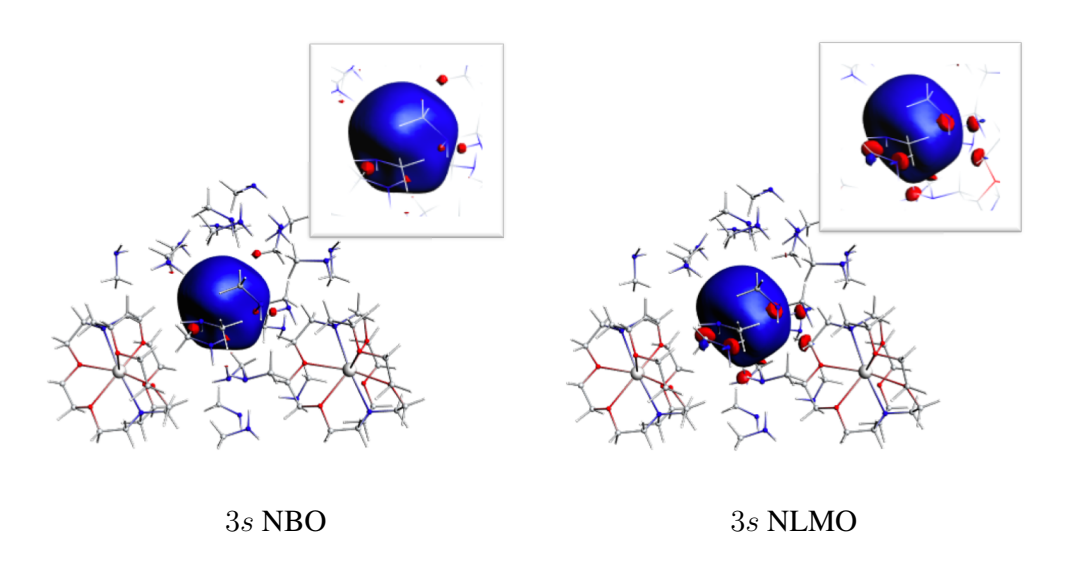


Figure 5: Isosurface (±0.022 au) of the 3s NBO and NLMO for Na of snapshot 4.

For the Na⁻ ion, the analysis shows a somewhat larger spread of V_{33} values than the Na⁺ analysis, in line with Figure 3. This reflects the more flexible environment of Na⁻ (solvent and cryptands) compared to Na⁺, which is encapsulated in the cryptand. For the larger EFGs among the snapshots, the Diffuse + Other contributions have the same sign as the 2p contributions and can be attributed to the same core-polarization mechanism as found for Na⁺.

Across the snapshots, the diffuse nature of the 3s shell of Na⁻ causes the parent NBO to contribute only between 69 and 86% weight to the 3s NLMO, indicating a varying strong degree of delocalization. (Some of this may be enhanced by the delocalization error, as already mentioned. Additional calculated data addressing this point can be found in the SI.) Accordingly, the natural populations assigned to Na⁻ range between 11.4 and 11.7*e* instead of the formal 12 electrons. The deviation from the formal electron count of 12 correlates with a decreasing weight of the parent

NBO in the 3s NLMO. In other words, during the dynamics the sodide 3s electron density deforms and partially delocalizes into the solvation shell to varying degrees. As shown in Figure 5 for one of the snapshots, the 3s shell is visibly deformed, i.e. not at all free ion-like. In Table 2, the polarization is indicated by the weights of Na-centered p and d angular momenta in the 3s NLMO, which also correlate with the decreasing parent NBO weights.

When the Na⁻ 3s shell deforms and acquires p (and d) character, this may generate an EFG directly, via the aspherical electron density, and indirectly via a core polarization driven by the valence-core orthogonality. The analysis is not capable of separating the two mechanisms cleanly, but this hardly matters: The data in Table 2 show that the 3s contribution to the Na⁻ EFG is rarely comparable to the 2p contribution (usually smaller), and there is no systematic relation between the signs and magnitudes of the 3s and 2p contributions within the available data set.

These findings may be interpreted as follows:

- (i) The diffuse 3s shell of Na⁻ is only weakly coupled to the [Ne] core as far as the EFG is concerned.
- (ii) The diffuse 3s shell is not capable of generating a sizable EFG on its own despite the fact that it is very easily polarized.
- (iii) The weak coupling between 3s and the core shells, and the lack of a strong EFG from 3s itself, causes the 3s shell to act like a buffer between the core and the ion's surrounding, such that the EFG tensor components de-correlate quickly in the time domain. The fast de-correlation is evident from the calculated relaxation data. Very sharp ²³Na signals for Na⁻ appear as a consequence.

In conclusion, Na¯ does not necessarily behave like a quasi-free ion that interacts only weakly with its environment. Rather, the filled 3s shell of Na¯ interacts weakly with the ion's own core and the nucleus, making Na¯ to appear in NMR experiments like a free ion. We expect that similar conclusions can be drawn about the nuclear magnetic shielding (NMR chemical shift) of Na¯ as well, although sodide may hold further surprises. In the characterization of crystalline samples, Dye et al. report large distances from the anion to the neighboring atoms, and the solid-state NMR indicates that the quadrupolar relaxation for the sodite ion is similarly inefficient as it is in solution. ^{17,58} It is therefore very likely that the sodide nucleus is similarly decoupled from the valence shell in the solid structure as we find here for the liquid solution phase.

We plan to investigate the chemical shifts in the near future by aiMD calculations, along with other alkali metals. For instance, it seems possible that the NMR data of K⁻, Rb⁻, and Cs⁻ show a stronger sensitivity to the chemical environment because the outer core shells of heavier alkalides are more easily polarizable than the 'primogenic' 2p shell of sodite.

Acknowledgments

We acknowledge the Center for Computational Research (CCR) at the University at Buffalo for providing computational resources. This work has been supported by Grant CHE-1855470 from the National Science Foundation.

Supporting Information Available

EFG and relaxation data for the individual BLYP and PBE trajectories. Comparisons between PAW and STO calculations, as well as different functionals and basis sets. Relevant structural and dynamic analyses. Isosurfaces of selected NBO and NLMO for Na cation. Mulliken and natural charges for all the snapshots analyzed. Delocalization error analysis. NBO analysis of V_{33} contributions with different functionals and basis sets.

References

- (1) Dye, J. L. Anions of the Alkali Metals. *Sci. Am.* **1977**, 237, 92–107.
- (2) Dye, J. L.; DeBacker, M. G. Physical and Chemical Properties of Alkalides and Electrides. *Annu. Rev. Phys. Chem.* **1987**, *38*, 271–299.
- (3) Wagner, M. J.; Dye, J. L. Alkalides, Electrides, and Expanded Metals. *Annu. Rev. Mat. Sci.* **1993**, *23*, 223–253.
- (4) Dye, J. L. Compounds of Alkali Metal Anions. Angew. Chem. Int. Ed. 1979, 18, 587–598.
- (5) Tehan, F. J.; Barnett, B. L.; Dye, J. L. Alkali Anions. Preparation and Crystal Structure of a Compound which Contains the Cryptated Sodium Cation and the Sodium Anion. *J. Am. Chem. Soc.* **1974**, *96*, 7203–7208.
- (6) Sokol, M.; Grobelny, J.; Grobelny, Z.; Stolarzewicz, A. Relaxation Study of Potassium Anions and Cations in Tetrahydrofuran Containing 15-Crown-5 by Potassium-39 NMR. *J. Phys. Chem.* **1993**, *97*, 763–766.
- (7) DeBacker, M. G.; Mkadmi, E. B.; Sauvage, F. X.; Lelieur, J.-P.; Wagner, M. J.; Concepcion, R.; Kim, J.; McMills, L. E. H.; Dye, J. L. The Lithium-Sodium-Methylamine System: Does a Low-Melting Sodide Become a Liquid Metal?. *J. Am. Chem. Soc.* **1996**, *118*, 1997–2003.

- (8) Edwards, P. P.; Ellaboudy, A. S.; Holton, D. M.; Pyper, N. The Chemical Dynamics of Nain Liquid 12-Crown-4 Solutions Deduced from 23Na Nuclear Spin Relaxation Rates. *Mol. Phys.* **1990**, *69*, 209–227.
- (9) Kim, J.; Eglin, J. L.; Ellaboudy, A. S.; McMills, L. E. H.; Huang, S.; Dye, J. L. 87Rb, 85Rb, and 39K NMR Studies of Alkalides, Electrides, and Related Compounds. *J. Phys. Chem.* **1996**, *100*, 2885–2891.
- (10) Zurek, E. Alkali Metals in Ethylenediamine: A Computational Study of the Optical Absorption Spectra and NMR Parameters of $[M(en)_3^+ \cdot M^-]$ Ion-Pairs. *J. Am. Chem. Soc.* **2011**, *133*, 4829–4839.
- (11) Ceraso, J. M.; Dye, J. L. 23Na NMR Spectrum of the Sodium Anion. *J. Chem. Phys.* **1974**, *61*, 1585–1587.
- (12) Dye, J. L.; Andrews, C. W.; Ceraso, J. M. Nuclear Magnetic Resonance Studies of Alkali Metal Anions. *J. Phys. Chem.* **1975**, *79*, 3076–3079.
- (13) Dye, J.; Ellaboudy, A.; Kim, J. *Modern NMR Techniques and Their Application in Chemistry;* Marcel Dekker, Inc.: New York, 1991.
- (14) Ellaboudy, A.; Dye, J. L. Lineshapes in Sodium-23 NMR Spectra of Crystalline Sodides. *J. Mag. Res.* **1986**, *66*, 491–502.
- (15) Phillips, R. C.; Khazaeli, S.; Dye, J. L. Sodium-23 Nuclear Magnetic Resonance Study of Sodium Metal in Methylamine Solutions That Contain 18-Crown-6. Kinetics of Sodium Cation-Sodide Ion Exchange. *J. Phys. Chem.* **1985**, *89*, 606–612.
- (16) Pyper, N. C.; Edwards, P. P. Nuclear Shielding in the Alkali Metal Anions. *J. Am. Chem. Soc.* **1986**, *108*, 78–81.
- (17) Kim, J.; Dye, J. L. Single-Crystal Sodium-23 NMR Study of (Cryptand [2.2.2]) Sodium(1+) Sodide. *J. Phys. Chem.* **1990**, *94*, 5399–5402.
- (18) Edwards, P. P.; Ellaboudy, A. S.; Holton, D. M. NMR Spectrum of the Potassium Anion K-. *Nature* **1985**, *317*, 242–244.
- (19) Ellaboudy, A. S.; Holton, D. M.; Pyper, N. C.; Edwards, P. P.; Wood, B.; McFarlane, W. Gas-Like Nature of the Sodium Anion in Solution. *Nature* **1986**, *321*, 684–685.
- (20) Spiess, H. W. Rotation of Molecules and Nuclear Spin Relaxation. In *NMR Basic Principles and Progress*, Vol. 15; P. Diehl, R. K. E. Fluck, Ed.; Springer: Berlin, 1978 55–214.

- (21) Cowan, B. *Nuclear Magnetic Resonance and Relaxation;* Cambridge University Press: Cambridge, UK, 2005.
- (22) Kowalewski, J.; Mäler, L. Nuclear Spin Relaxation in Liquids: Theory, Experiments, and Applications; Taylor & Francis: New York, 2006.
- (23) Pyper, N. C.; Pike, C. G.; Edwards, P. P. Polarizability and Nuclear Shielding for the Sodium Anion in Condensed Phases. *J. Am. Chem. Soc.* **1993**, *115*, 1468–1478.
- (24) Matalon, S.; Golden, S.; Ottolenghi, M. Nature of the Visible Absorption Bands in Metal-Amine Solutions. *J. Phys. Chem.* **1969**, *73*, 3098–3101.
- (25) Roberts, J. E.; Schnitker, J. Ionic Quadrupolar Relaxation in Aqueous Solution: Dynamics of the Hydration Sphere. *J. Phys. Chem.* **1993**, *97*, 5410–5417.
- (26) Aidas, K.; Ågren, H.; Kongsted, J.; Laaksonen, A.; Mocci, F. A Quantum Mechanics/Molecular Dynamics Study of Electric Field Gradient Fluctuations in the Liquid Phase. The Case of Na⁺ in Aqueous Solution. *Phys. Chem. Chem. Phys.* **2013**, *15*, 1621–31.
- (27) Badu, S.; Truflandier, L. A.; Autschbach, J. Quadrupolar NMR Spin Relaxation Calculated Using Ab-initio Molecular Dynamics: Group 1 and Group 17 Ions in Aqueous Solution. *J. Chem. Theory Comput.* **2013**, *9*, 4074–4086.
- (28) Carof, A.; Salanne, M.; Charpentier, T.; Rotenberg, B. Accurate Quadrupolar NMR Relaxation Rates of Aqueous Cations from Classical Molecular Dynamics. *J. Phys. Chem. B* **2014**, *118*, 13252–13257.
- (29) Philips, A.; Marchenko, A.; Truflandier, L. A.; Autschbach, J. Quadrupolar NMR Relaxation from Ab-Initio Molecular Dynamics: Improved Sampling and Cluster Models vs. Periodic Calculations. *J. Chem. Theory Comput.* **2017**, *13*, 4397–4409.
- (30) Schmidt, J.; Hutter, J.; Spiess, H.-W.; Sebastiani, D. Beyond Isotropic Tumbling Models: Nuclear Spin Relaxation in Liquids from First Principles. *ChemPhysChem* **2008**, *9*, 2313–2316.
- (31) Philips, A.; Marchenko, A.; Ducati, L. C.; Autschbach, J. Quadrupolar ¹⁴N NMR Relaxation from Force-Field and Ab-Initio Molecular Dynamics in Different Solvents. *J. Chem. Theory Comput.* **2019**, *15*, 509–519.
- (32) Giannozzi, P.; Baroni, S.; Bonini, N.; Calandra, M.; Car, R.; Cavazzoni, C.; Ceresoli, D.; Chiarotti, G. L.; Cococcioni, M.; Dabo, I. *et al.* QUANTUM ESPRESSO: A Modular and

- Open-Source Software Project for Quantum Simulations of Materials. *J. Phys. Cond. Mat.* **2009**, *21*, 395502.
- (33) Giannozzi, P.; Andreussi, O.; Brumme, T.; Bunau, O.; Nardelli, M. B.; Calandra, M.; Car, R.; Cavazzoni, C.; Ceresoli, D.; Cococcioni, M. *et al.* Advanced Capabilities for Materials Modelling with Quantum ESPRESSO. *J. Phys. Cond. Mat.* **2017**, *29*, 465901.
- (34) Biswas, S.; Mallik, B. S. Time-Dependent Vibrational Spectral Analysis of First Principles Trajectory of Methylamine with Wavelet Transform. *Phys. Chem. Chem. Phys.* **2017**, *19*, 9912–9922.
- (35) Becke, A. D. Density-Functional Exchange-Energy Approximation with Correct Asymptotic Behavior. *Phys. Rev. A* **1988**, *38*, 3098–3100.
- (36) Lee, C.; Yang, W.; Parr, R. G. Development of the Colle-Salvetti Correlation-Energy Formula into a Functional of the Electron Density. *Phys. Rev. B* **1988**, *37*, 785–789.
- (37) Dal Corso, A. Pseudopotentials Periodic Table: From H to Pu. *Comput. Mater. Sci.* **2014**, 95, 337–350.
- (38) Grimme, S.; Antony, J.; Ehrlich, S.; Krieg, H. A Consistent and Accurate Ab Initio Parametrization of Density Functional Dispersion Correction (DFT-D) for the 94 Elements H-Pu. *J. Chem. Phys.* **2010**, *132*, 154104.
- (39) DiStasio Jr., R. A.; Santra, B.; Li, Z.; Wu, X.; Car, R. The Individual and Collective Effects of Exact Exchange and Dispersion Interactions on the Ab Initio Structure of Liquid Water. *J. Chem. Phys.* **2014**, *141*, 84502.
- (40) Marchenko, L. A. Truflandier; Autschbach, J. Uranyl Carbonate Complexes in Aqueous Solution and Their Ligand NMR Chemical Shifts and ¹⁷O Quadrupolar Relaxation Studied by Ab Initio Molecular Dynamics. *Inorg. Chem.* **2017**, *56*, 7384–7396.
- (41) Truflandier, L. A.; Autschbach, J. Probing the Solvent Shell with 195Pt Chemical Shifts: Density Functional Theory Molecular Dynamics Study of PtII and PtIV Anionic Complexes in Aqueous Solution. *J. Am. Chem. Soc.* **2010**, *132*, 3472–3483.
- (42) TINKER Software Tools for Molecular Design by J. W. Ponder.
- (43) Perdew, J. P.; Burke, K.; Ernzerhof, M. Generalized Gradient Approximation Made Simple. *Phys. Rev. Lett.* **1996**, *77*, 3865–3868.

- (44) Blöchl, P. E. Projector Augmented-Wave Method. *Phys. Rev. B* **1994**, *50*, 17953–17979.
- (45) Marchenko, A.; Duignan, T.; Philips, A.; Badger, G.; Ludowieg, H. D.; Moore, B. "Exatomic: A Unified Platform for Computational Chemists", doi:10.5281/zenodo.595724.
- (46) Baerends, E. J.; Ziegler, T.; Autschbach, J.; Bashford, D.; Bérces, A.; Bickelhaupt, F. M.; Bo, C.; Boerrigter, P. M.; Cavallo, L.; Chong, D. P. *et al.* "Amsterdam Density Functional, SCM, Theoretical Chemistry, Vrije Universiteit, Amsterdam, The Netherlands.".
- (47) Adamo, C.; Barone, V. Toward Reliable Density Functional Methods without Adjustable Parameters: The PBE0 Model. *J. Chem. Phys.* **1999**, *110*, 6158–6170.
- (48) Klamt, A.; Schüürmann, G. COSMO: A New Approach to Dielectric Screening in Solvents with Explicit Expressions for the Screening Energy and Its Gradient. *J. Chem. Soc. Perkin Trans.* 2 **1993**, 799–805.
- (49) Cohen, A. J.; Mori-Sánchez, P.; Yang, W. Challenges for Density Functional Theory. *Chem. Rev.* **2012**, *112*, 289–320.
- (50) Autschbach, J.; Srebro, M. Delocalization Error and 'Functional Tuning' in Kohn-Sham Calculations of Molecular Properties. *Acc. Chem. Res.* **2014**, *47*, 2592–2602.
- (51) Srebro, M.; Autschbach, J. Does a Molecule-Specific Density Functional Give an Accurate Electron Density? The Challenging Case of the CuCl Electric Field Gradient. *J. Phys. Chem. Lett.* **2012**, *3*, 576–581.
- (52) Schwerdtfeger, P.; Pernpointner, M.; Nazarewicz, W. Calculation of Nuclear Quadrupole Coupling Constants. In *Calculation of NMR and EPR Parameters. Theory and Applications*; Kaupp, M.; Bühl, M.; Malkin, V. G., Eds.; Wiley-VCH: Weinheim, 2004 279–291.
- (53) Sit, P. H.-L.; Marzari, N. Static and Dynamical Properties of Heavy Water at Ambient Conditions from First-Principles Molecular Dynamics. *J. Chem. Phys.* **2005**, *122*,.
- (54) Autschbach, J.; Zheng, S.; Schurko, R. W. Analysis of Electric Field Gradient Tensors at Quadrupolar Nuclei in Common Structural Motifs. *Concepts Magn. Reson. A* **2010**, *36A*, 84–126.
- (55) Perras, F. A.; Bryce, D. L. Multinuclear Magnetic Resonance Crystallographic Structure Refinement and Cross-Validation Using Experimental and Computed Electric Field Gradients: Application to Na2Al2B2O7. *J. Phys. Chem. C* 2012, *116*, 19472–19482.

- (56) Perras, F. A.; Korobkov, I.; Bryce, D. L. NMR Crystallography of Sodium Diphosphates: Combining Dipolar, Shielding, Quadrupolar, Diffraction, and Computational Information. *CrystEngComm* **2013**, *15*, 8727–8738.
- (57) Glendening, E. D.; Badenhoop, J. K.; Reed, A. E.; Carpenter, J. E.; Bohmann, J. A.; Morales, C. M.; Weinhold, F. "NBO 5.0", Theoretical Chemistry Institute, University of Wisconsin, Madison, 2001.
- (58) Dye, J. L.; Ceraso, J. M.; Lok, M.; Barnett, B. L.; Tehan, F. J. Crystalline Salt of the Sodium Anion (Na-). *J. Am. Chem. Soc.* **1974**, *96*, 608–609.